

國立臺灣大學生農學院生物產業機電工程學系



碩士論文

Department of Bio-Industrial Mechatronics Engineering

College of Bioresources and Agriculture

National Taiwan University

Master Thesis

以三維影像處理方法量化與分析大岩桐花朵形狀變異

Three-dimensional Approach for Quantifying and
Analyzing Floral Shape Variation in *Sinningia speciosa*

王政鈞

Cheng-Chun Wang

指導教授：郭彥甫 博士

Advisor: Yan-Fu Kuo, Ph.D.

中華民國 104 年 7 月

July, 2015

ACKNOWLEDGEMENTS



I would like to express my sincere gratefulness to Professor Yan-Fu Kuò, my research advisor, for his guidance and assistance during my master degree. I would also like to thank Hao-Chun for his support in biological knowledge I was not familiar with. I am grateful to Professor Chun-Neng Wang and his team for providing floral samples used in my research. I would like to appreciate Dr. W.-J. Chang for providing the equipment to acquire three-dimension flower images. I am grateful to my Lab304 members, Cheng-Liang, Wei-Tung, Tzu-Kuei, Walter, Han, Jerry, Andrew, David, Robert, Gado and Erica, who had accompanied me during my master degree. Lastly, I am deeply grateful to my family, especially my parents for their support throughout my study.

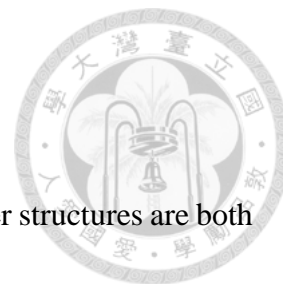
摘要



由於花朵的構造相當多變且複雜程度也很高，量化花朵形狀變異是件很困難的任務。以往花朵形狀變異是在二維照片上面以線性量測方法量化，由於二維照片無法充分地描述花朵構造，因此在量化花朵形狀變異上會有辨識不夠清楚的地方，因此此研究以斷層掃描照射花朵建構出花朵三維影像且以幾何形態方法分析三維花朵形狀變異，為了顯示出此研究所提出三維幾何形態分析方法的好處，此方法所應用的對象為大岩桐第二子代的花朵，第一子代花朵由兩側對稱和輻射對稱的親本雜交培育出來的花朵，第二子代花朵為第一子代花朵自交而成，此第二子代花朵不論在大小或是形狀變異上都呈現極大差異，因此作為量化表現型的研究是很好的研究材料，試驗過程中以影像處理強化由斷層掃描得到的三維花朵影像，接著選取特徵點以供接下來幾何形態分析所需，每朵花選取95個同源特徵點作為花朵形狀的描述，如此一來不但能增加對於花朵的描述也更能說明花朵的形狀變異。試驗結果說明花瓣裂片的向外開合程度還有花冠筒對稱性為主要的花朵形態變異。此研究所提出以斷層掃描得到三維花朵影像並以三維幾何形態來量化花朵形狀的方法，所得到的結果不但能截取出許多在二維影像上無法截取到的形狀變異特徵，在量化形狀變異上也更加精確。除此之外不同花瓣在幾何形態上的共變程度也能透過不同花瓣的特徵點進行轉置檢驗來分析。分析結果顯示背部花瓣和腹部花瓣共變程度為最小，有可能可視為不同模組。

關鍵字：花朵形態變異，幾何形態，斷層掃描，普氏分析，主成分分析，模塊化和整合

ABSTRACT



The quantification of floral shape variations is difficult because flower structures are both diverse and complex. Traditionally, floral shape variations are quantified using linear measurements of two-dimensional (2D) images. The 2D images cannot adequately describe flower structures, and thus lead to unsatisfactory discrimination of the flower shape. This study aimed to acquire three-dimensional (3D) images by using micro-computed tomography (μ CT) and to examine the floral shape variations by using geometric morphometrics (GM). To demonstrate the advantages of the 3D- μ CT-GM approach, we applied the approach to a second-generation (F_2) population of *Sinningia speciosa* crossed from parents of zygomorphic and actinomorphic flowers. The flowers in the F_2 population considerably vary in size and shape, thereby served as good materials to test the applicability of the proposed phenotyping approach. Procedures were developed to improve the quality of 3D volumetric flower images acquired using a μ CT scanner and to select homologous characteristic points (i.e., landmarks) from the flower images for the subsequent GM analysis. The procedures identified 95 landmarks for each flower and thus improved the overall quality of describing and illustrating the flower shapes. The GM analysis demonstrated that flower opening and dorsoventral symmetry were the principal shape variations of the flowers. The 3D- μ CT-GM approach revealed shape variations that could not be identified using typical 2D approaches and accurately

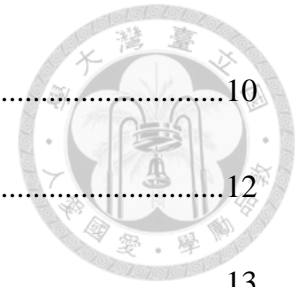
quantified the flower traits that presented a challenge in 2D images. In addition, the level of morphological integration between the petal landmark sets were examined by using permutation tests. The tests indicated that dorsal and ventral petals were associated with a minimal level of integration and could be regarded as biological modules.

Keywords: floral shape variation, geometric morphometrics (GM), computed tomography (CT), generalized Procrustes analysis (GPA), principal component analysis (PCA), modularity and integration

TABLE OF CONTENTS

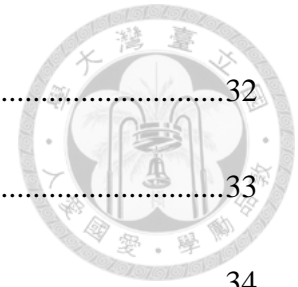


ACKNOWLEDGEMENTS	i
摘要	ii
ABSTRACT	iii
TABLE OF CONTENTS	v
LIST OF FIGURES	viii
CHAPTER 1. INTRODUCTION.....	1
1.1 Quantification of Flower Shape Variation.....	1
1.2 Morphological Integration.....	1
1.3 Objectives	2
1.4 Organization	3
CHAPTER 2. LITERATURE REVIEW	5
2.1 Classic Morphometrics and Geometric Morphometrics.....	5
2.2 GM Using Three Dimension Image	6
2.3 Morphological Integration between Compartments	7
CHAPTER 3. QUANTIFICATION OF FLORAL SHAPE IN THREE-DIMENSION...8	
3.1 Material and Methods.....	9
3.1.1 Flower material.....	9
3.1.2 Floral image acquisition	10



3.1.3 Quality improvement of flower images.....	10
3.1.4 Landmark identification	12
3.1.5 Shape variation quantification	13
3.1.6 Major morphological traits	14
3.2 Results	14
3.2.1 Three-dimensional flower images and landmarks.....	14
3.2.2 Identification and visualization of floral shape variations.....	15
3.2.3 Morphological traits: flower opening and corolla asymmetry	20
3.2.4 Transition between the zygomorphic and actinomorphic flowers.....	22
3.2.5 Comparison of shape variation analyses performed using 2D and 3D images.....	23
3.4 Discussion.....	27
3.4.1 Advantages of 3D floral shape analysis	27
3.4.2 Reasons for 3D analysis outperforming 2D analysis	28
3.4.3 Biological implications of flower shape variations	29
3.5 Concluding Remarks	30
CHAPTER 4. MORPHOLOGICAL INTEGRATION BETWEEN FLORAL PETALS FOR <i>SINNINGIA SPECIOSA</i>	31
4.1 Material and Methods.....	32

4.1.1 Flower compartments	32
4.1.2 Test of morphological integration	33
4.2 Results	34
4.2.1 Morphological integration	34
4.3 Concluding Remarks	38
CHAPTER 5. CONCLUSIONS	39
REFERENCES	40



LIST OF FIGURES



Figure 1. Side-view images of (A) a trumpet-shaped zygomorphic flower and (B) a tubular-shaped actinomorphic flower from an intercross line of *Sinningia speciosa*.3

Figure 2. Interbreeding process of *S. speciosa* flowers.9

Figure 3. (A) Volumetric image, (B) surface image, and (C) flower landmarks.11

Figure 4. Primary and secondary landmarks on a petal.....13

Figure 5. (A) Image of a flower, (B) corresponding μ CT image, and (C) landmarks on the flower image.....15

Figure 6. Scatter plots of the first three principal components.....16

Figure 7. Illustration of flower shape variations caused by changes in PCs.17

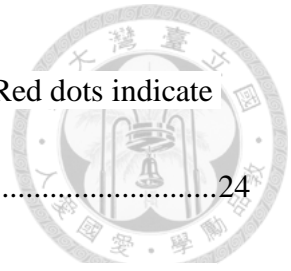
Figure 8. (A) Front-view and (B) side-view illustration of the flower shape variations..19

Figure 9. (A) Tube-opening and lobe-widening circles for calculating the opening score and (B) the asymmetry angle.....21

Figure 10. Scatter plots of (A) PC1 and flower opening, and (B) PC2 and the asymmetry score.....22

Figure 11. (A) Flower of the smallest opening value, (B) histogram of flower opening, (C) flower of the largest opening value, (D) flower of the smallest corolla asymmetry, (E) histogram of corolla asymmetry, and (F) flower of the largest corolla asymmetry.. 23

Figure 12. 2D (A) front-view and (B) side-view images of a flower. Red dots indicate landmarks selected along the contours.	24
Figure 13. (A) Front-view and (B) side-view illustrations of the floral shape variation quantified using 2D images.	26
Figure 14. Compartments of landmarks. (A) compartments of petals (B) compartments of tubes.	32
Figure 15. Null distributions of the permutation tests for first compartment set.	36
Figure 16. Null distributions of the permutation tests for second compartment set.	37



CHAPTER 1. INTRODUCTION



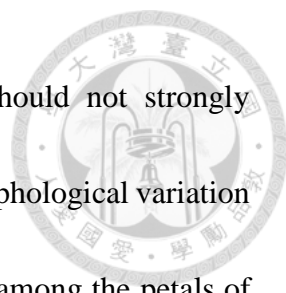
1.1 Quantification of Floral Shape Variation

Flowers are essential organs for reproduction in angiosperms. The flower shape can vary tremendously. The morphological variations in the corolla must be determined quantitatively to address questions regarding evolutionary divergence (Gómez et al., 2006; Feng et al., 2009), genotype–phenotype association (Cui et al., 2010; Hsu et al., 2015) plant–pollinator interactions (Yoshioka et al., 2005; Galliot et al., 2006; Gomez et al., 2008), and breeding selection (Yoshioka et al., 2006; Kobayashi et al., 2007; Kawabata et al., 2009; Kanaya et al., 2010). We proposed an approach to quantify the shape variations of corollas in three-dimensional (3D) images by using micro-computed tomography (μ CT) and geometric morphometrics (GM).

1.2 Morphological Integration

Morphological integration of floral petal development is intriguing to botanists. Morphological integration refers to the tendency of compartments (e.g., petals) of an organism to illustrate correlation in shape variation (Olson and Miller, 1958). A corolla typically consists of several petals. These petals can develop integrally as a whole or can establish separately from each other as independent modules.

Morphological integration is typically measured by the level of covariation among compartment structures (Klingenberg et al., 2001). If petals do not show the tendency to



vary coordinately in shape, the structural variation of a petal should not strongly correlated to the structural variation of another petal. Instead, the morphological variation occurs primarily within the petals. Hence, the degree of covariation among the petals of a corolla is low, and the petals more likely develop independently. These petals than can be considered as biological modules (Klingenberg, 2009). The incoordination among petal development can result in appreciable corolla shape variation (e.g., dorsoventral asymmetry).

1.3 Objectives

We proposed a procedure to quantify and analyze corolla shape variations in 3D images by using μ CT, GM, and image processing. The procedure was applied to the flowers of the F₂ population resulting from an intercross between a zygomorphic variety and an actinomorphic cultivar of *Sinningia speciosa* (Hsu et al., 2015). These F₂ flowers showed a considerable degree of variation in flower opening and corolla symmetry (Fig. 1), thus serving as excellent materials for performing the quantification of floral shape variations and studying the issue of morphological integration of petals. The specific objectives of our study were to: (1) identify the leading morphological variations of flowers; (2) define and quantify physically measured traits such as flower opening and corolla asymmetry; (3) observe the floral shape transition between the zygomorphic and actinomorphic flowers; (4) compare the floral shape analysis results obtained using 3D images with those

obtained using 2D images; (5) examine the degree of morphological integration between petals of the flowers.

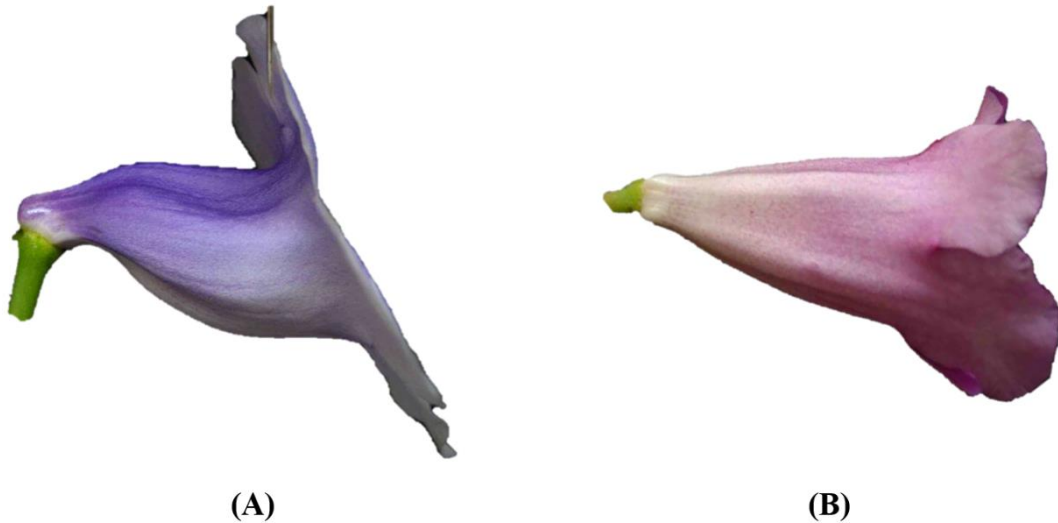


Figure 1. Side-view images of (A) a trumpet-shaped zygomorphic flower and (B) a tubular-shaped actinomorphic flower from an intercross line of *Sinningia speciosa*.

1.4 Organization

The remaining of this document is organized as follows. In Chapter 2, some previous studies which analyzed morphological variance of studied objects, three dimension image for objects, and morphological integration between compartments were reviewed. Two types of morphometrics, which were classic morphometrics and geometric morphometrics, were introduced and compared. In Chapter 3, 3D floral images scanned by micro-computed tomography (μ CT) were used to accurately quantify floral shape variation through three dimension GM. The results of 3D GM were compared to 2D GM. In Chapter 4, flower petals of *S. speciosa* were divided into three compartments: dorsal,

lateral, and ventral petals. The level of morphological integration for the compartments were examined. Conclusions of this research are given in Chapter 5.



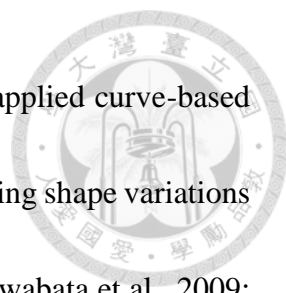
CHAPTER 2. LITERATURE REVIEW



2.1 Classic Morphometrics and Geometric Morphometrics

The analysis of floral shape discrepancies is traditionally performed using classic morphometrics (Miller and Venable, 2003; Pérez et al., 2004; Kobayashi et al., 2007; Fernández-Mazuecos et al., 2013; Wessinger et al., 2014). Classic morphometrics uses multivariate statistics to measure distances between morphological landmarks (i.e., characteristic points). The differences in distances between specimens are then evaluated. Shape is mathematically defined as the geometric information of an object except its scaling, translation, and rotation (Gower, 1975). Determining the distances between the landmarks neither reconstructs the original geometric relationship nor separates the shape information from the overall size of the specimens. Thus, the classic morphometrics approach has been considered less amenable in studies of floral shape variations (Dalayap et al., 2011; Fernández-Mazuecos et al., 2013).

Geometric morphometrics (GM; Zelditch et al., 2004; Lawing and Polly, 2010) has been increasingly used to quantify the flower shape because of the recent advances in digital photography (Dalayap et al., 2011; Savriama et al., 2012). GM is a collection of algorithms that convey the spatial correlation on a set of landmarks identified from the photographic images of the objects to be analyzed. The method preserves the geometries of the landmark configurations. Thus, the statistical results of GM can describe the actual



shape or form divergences. In recent years, numerous studies have applied curve-based GM techniques (Kuhl and Giardina, 1982; Bo et al., 2014) for evaluating shape variations of individual petals (Yoshioka et al., 2005; Yoshioka et al., 2007; Kawabata et al., 2009; Kawabata et al., 2011; Nii and Kawabata, 2011). Some other studies have used landmark-based GM techniques (Adams et al., 2004; Klingenberg, 2010) for examining the morphological divergence of corollas (Shipunov et al., 2004; Gómez et al., 2006; Gomez et al., 2008; Feng et al., 2009; Kaczorowski et al., 2012; Savriama et al., 2012; Hsu et al., 2015).

2.2 GM Using Three Dimension Image

Recent advances in modern scanning techniques make it feasible and affordable to reconstruct 3D images for objects. Typically, volumetric data on delicate botanical materials (e.g., flowers) are obtained using computed tomography or magnetic resonance image scanners. Furthermore, the high resolution of these technologies provides the detailed information required for accurately quantifying morphological variations. Studies have applied these 3D techniques to derive the shape equation for tomato (Li et al., 2011), perform vascular anatomy on living plants (McElrone et al., 2013), visualize the structural changes occurring in plant leaves (Pajor et al., 2013), and study the pollination syndromes of *Satyrium* flowers (van der Niet et al., 2010).

2.3 Morphological Integration between Compartments

The level of covariation among compartments was typically quantified and evaluated by using GM. GM is a collection of algorithms that examine shape variation on a set of landmarks of the objects to be studied. A number of studies have adopted GM approaches to examine morphological integration between compartments, including the forewings and hindwings of bumblebees (Klingenberg et al., 2001), the anterior and posterior of *Drosophila* wing (Klingenberg and Zaklan, 2000), the face and braincase of birds skulls (Klingenberg and Marugán-Lobón, 2013), the arterial Circle of Willis and skull of laboratory mice (Jamniczky and Hallgrímsson, 2011), the face and cerebral capsule of human cranial skeletons (Mitteroecker and Bookstein, 2008), and the vault, face, and cranial base of human skulls (Bookstein et al., 2003).



CHAPTER 3. QUANTIFICATION OF FLORAL SHAPE IN THREE-DIMENSION



This chapter proposes a method to quantify the floral shape variations in an F_2 cross of *Sinningia speciosa* by using 3D GM. Image processing algorithms were used to construct 3D floral images and improve the images quality. GM including generalized Procrustes analysis and principal component analysis were performed to evaluate the floral shape variation. The GM analysis demonstrated that corolla curvature, flower opening, and dorsoventral symmetry were principal shape variations of the flowers. To quantify the extent of flower opening due to curvature and the degree of corolla asymmetry, two traits — flower opening and corolla asymmetry were defined and quantified from the 3D floral images. The 3D GM method proposed in this chapter was compared to typical 2D GM. The 3D analysis was shown to be capable of observing shape variation that could not be identified by typical 2D approaches. The 3D GM approach opens new avenues to investigate floral shape variations.



3.1 Material and Methods

3.1.1 Flower material

The flower samples were obtained by crossing two cultivars of *S. speciosa*, “Carangola” and “Peridots Darth Vaders” (Fig. 2). These parental accessions were crossed to breed F₁ plants. The F₂ plants were generated by selfing a single F₁ plant. All plants were grown in a greenhouse under natural lighting with 20% shade and 70%–80% humidity at 22–28°C. We included only the flowers of the F₂ plants with exactly 5 petal lobes because the flowers with different numbers of petal lobes were incomparable in shape (i.e., nonhomologous; Adams et al., 2004) and thus should be excluded from comparison. The flower samples were provided by Prof. Chun-Neng Wang and his team in the Institute of Ecology and Evolutionary Biology at the National Taiwan University.

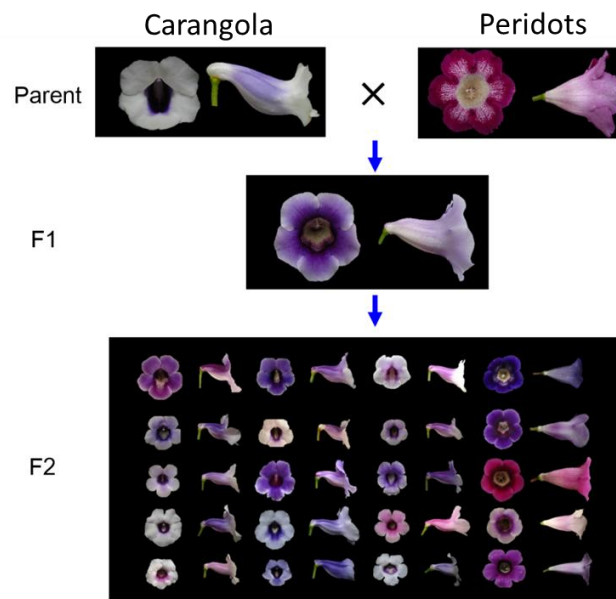


Figure 2. Interbreeding process of *S. speciosa* flowers.



3.1.2 Floral image acquisition

Three-dimensional flower images were acquired using a μ CT scanner (SkyScan 1076, Bruker, Kontich, Belgium). The specimens of first-day fully bloomed fresh flowers were cut at the stalk near the bottom of the tube and placed in the scanner chamber. The specimens were fastened to the base in the chamber with gummed tape to prevent the movement of the specimens during scanning. The transverse diameter of the chamber was 68 mm and the single scan length was 20 mm in the travel direction. The number of scans was dependent on the flower sizes. The X-ray source voltage, current, exposure time, and scanning resolution were set to 40 kV, 250 μ A, 150 ms, and 35 μ m, respectively. After scanning was completed, the 3D raw images were reconstructed by using SkyScan NRecon (Bruker, Kontich, Belgium). We acquired 57 flower images from various F_2 plants. The acquisitions were performed between August, 2012 and September, 2014.

3.1.3 Quality improvement of flower images

The raw images comprised flower specimens and the base for fastening the flower samples. Image processing algorithms were applied to segment the flowers from the background, reduce the noise of the images, and transform the images into an appropriate format for the subsequent analysis. During the process, the spatial resolution of the raw images was reduced by 50% to a voxel size of 70 μ m on each side to expedite processing.

The algorithms were implemented on the 2D slices of the 3D raw images along the travel direction. Region labeling (Haralick and Shapiro, 1992) was first applied to detect objects in the images. The base, the greatest object located at a fixed position in the slices, was automatically recognized and eliminated. The objects with pixel sizes smaller than a certain threshold (i.e., sparkles) were regarded as noise and were removed. The image contrast (i.e., gamma value) was adjusted appropriately to span the gray-level dynamic range. The resulting images, referred to as volumetric images (Fig. 3A), were then binarized. A morphological closing (Vincent, 1994) was applied to eliminate the hollow pixels within the flower petals. Surface images, which are composed of triangle meshes, were then generated (Hansen and Johnson, 2005; Fig. 3B). The mesh density was adjusted to maintain a reasonable resolution of the images. The image processing was performed using MATLAB (The Mathworks, Natick, MA, USA).

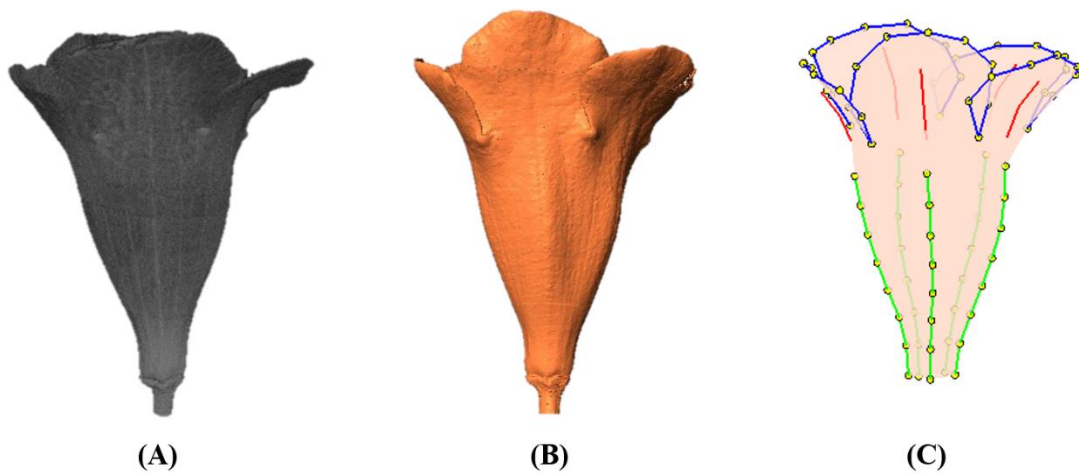


Figure 3. (A) Volumetric image, (B) surface image, and (C) flower landmarks.

3.1.4 Landmark identification



Landmarks are categorized as primary and secondary (Zelditch et al., 2004). In this study, the primary landmarks were defined as the anatomically recognizable points of the corolla, including the intersections of adjacent lobes, endpoints of petal midribs, and boundary points of lobes and tubes on petal midribs (solid dots in Fig. 4). The secondary landmarks were equally distributed points between the two primary landmarks along the lobe contours or petal midribs (hollow dots in Fig. 4). In the landmark identification process, the lobe contours and petal midribs were identified using the Landmark software (Wiley et al., 2005). The landmarks were then determined using a program developed in MATLAB. Thus, 95 landmarks, including 15 primary and 80 secondary, were collected for each specimen (Fig. 3C). The lobes and tubes comprised 55 and 50 landmarks, respectively, with 10 landmarks in common. *S. speciosa* and various angiosperm species natively develop flowers with limited anatomical points that can serve as the primary landmarks. The proposed approach for selecting the secondary landmarks in 3D images effectively increases the number of homologous characteristic points of the flowers being studied, and thus improving the overall quality of describing and illustrating the flower shapes.

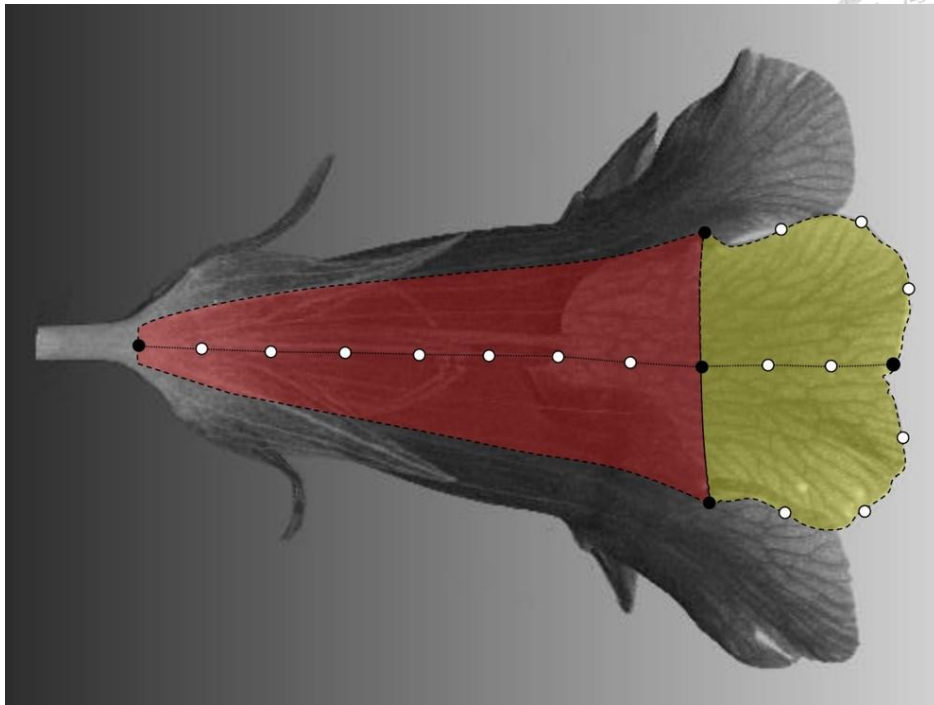


Figure 4. Primary and secondary landmarks on a petal.

3.1.5 Shape variation quantification

GM was applied to the landmarks for identifying the major shape variations between the flowers. The GM procedure includes generalized Procrustes analysis and principal component analysis (PCA; Zelditch et al., 2004; Lawing and Polly, 2010). Generalized Procrustes analysis was first implemented to eliminate variations mainly irrelevant to shape (e.g., shifting, rotating, and scaling). PCA was then applied to obtain few principal components (PCs) that accounted for a major portion of the landmark variability between the flowers. The major floral shape variations then could be visualized by reconstructing flowers by using inverse PCA with altered PC values.



3.1.6 Major morphological traits

The major shape variations identified by GM illustrated the transition between the zygomorphic and actinomorphic flowers. Morphological traits corresponding to the major shape variations were defined and quantified. These traits were physically measured in the volumetric images of the flowers using image processing and computer graphics and could genuinely and quantitatively represent the morphological characteristics of the flowers.

3.2 Results

3.2.1 Three-dimensional flower images and landmarks

Three-dimensional images of flowers were acquired. Image processing algorithms were used to segment the flower specimen from the background and to reduce noise in the images. Figure 5A and 5B show a flower image and its corresponding volumetric (μ CT) image. Landmarks were selected following the proposed procedure. Figure 5C shows the landmarks and their identification numbers.

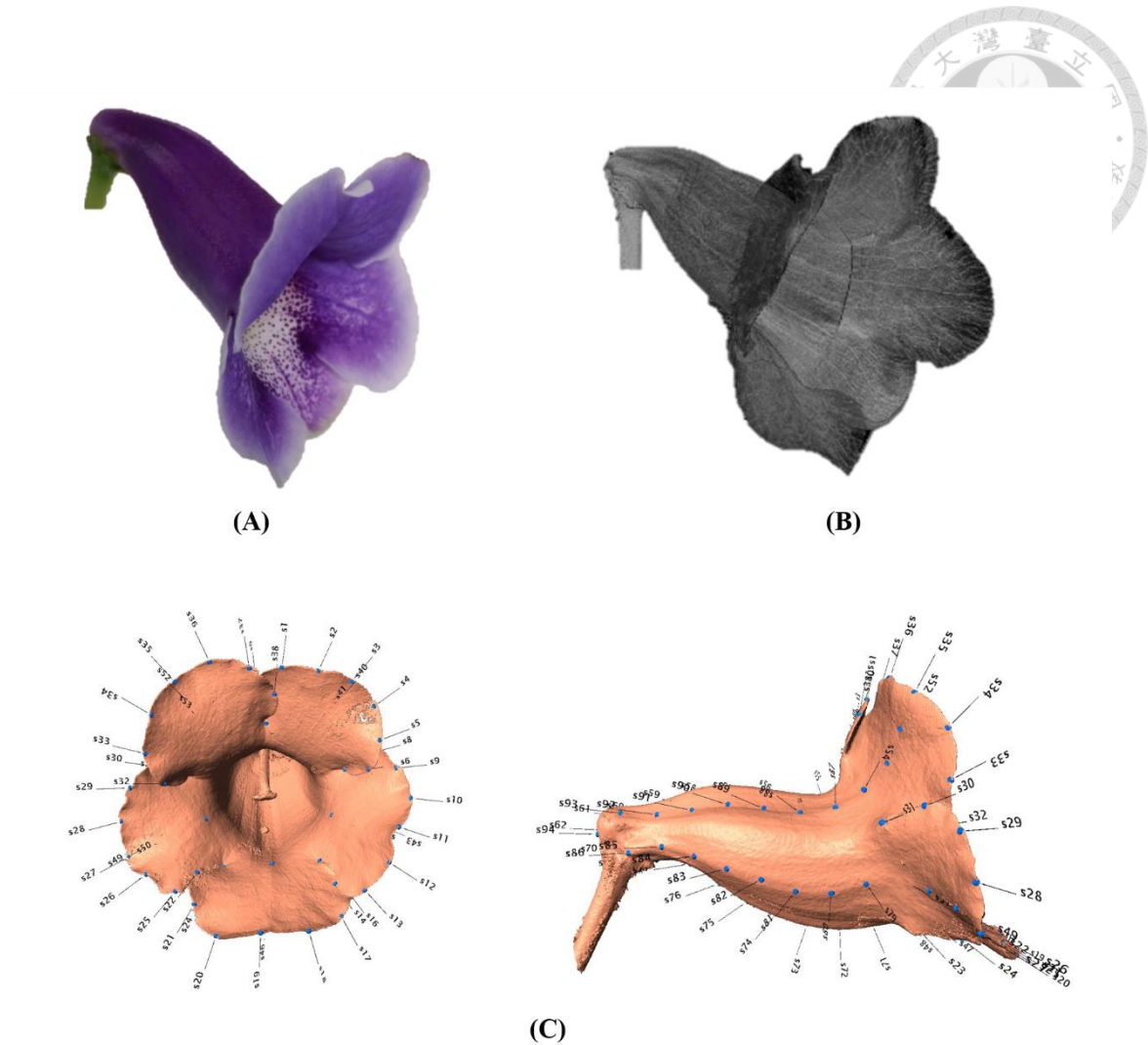


Figure 5. (A) Image of a flower, (B) corresponding μ CT image, and (C) landmarks on the flower image.

3.2.2 Identification and visualization of floral shape variations

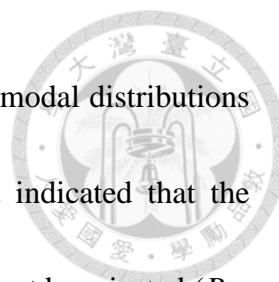
PCs describing the primary floral shape variations were derived. The first three PC scores,

PC1, PC2, and PC3, accounted for 38.8%, 16.3%, and 5.6% of the total shape variation.

Each of the remaining PC scores accounted for less than 4% of the total shape variation.

Because the first three PCs accumulated more than 60% of the total shape variation, we

presented the results of the first three PCs only. Figure 6 displays the scatter plots of PCs.



The PCs were standardized with zero means and unit variances. Unimodal distributions were observed for the first three PCs. Kolmogorov–Smirnov test indicated that the hypothesis that PC1, PC2, and PC3 were normally distributed could not be rejected ($P = 0.94, 0.84, \text{ and } 0.96$).

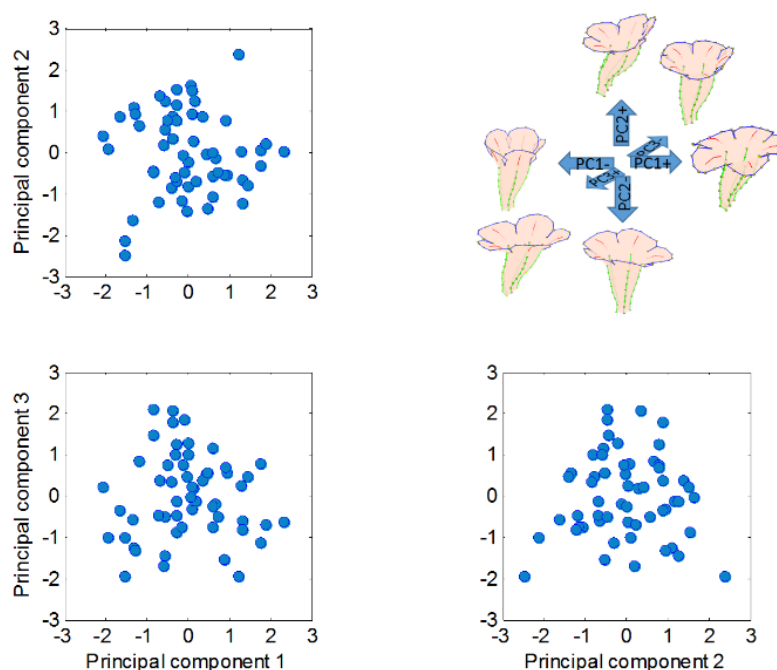
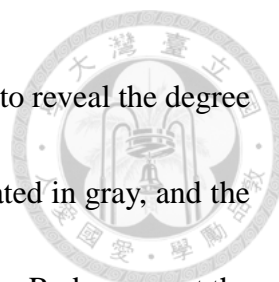


Figure 6. Scatter plots of the first three principal components.

Figure 7 illustrates the degree of floral shape variations caused by changes in the PCs. In the visualization process, the mean and standard deviation (STD) of the PCs were calculated. Reconstructed landmarks were calculated using an inverse PCA with a specific PC value being manipulated, whereas other PC values were maintained at mean values. The manipulated PC values were set at the mean or mean ± 2 STD. Flower shapes were then reconstructed using the resulting landmarks. The flowers were shown in 3D



images by using a thin-plate spline approach (Rohlf and Slice, 1990) to reveal the degree of shape transformation. In Figure 7, the mean flower shape is indicated in gray, and the reconstructed flowers with the manipulated PCs are illustrated in beige. Red arrows at the landmarks show the direction and degree of transformation from the mean shape to another. Major transformation was observed at the distal lobes (PC1 and PC2), boundary between the lobe and tube (PC2), margin between the tube and sepal (PC2), and tube chamber (PC3). Figure 8 shows the front (or face) and side views of the flowers.

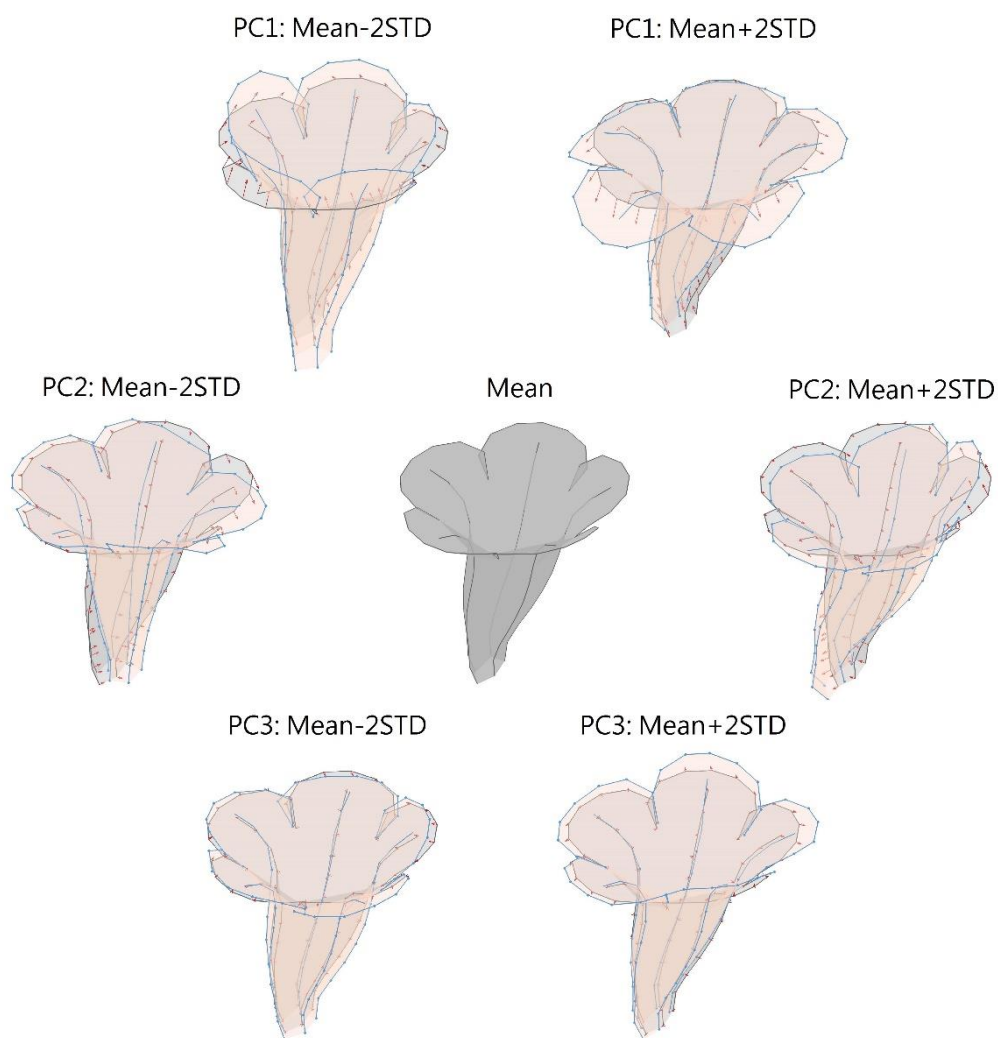
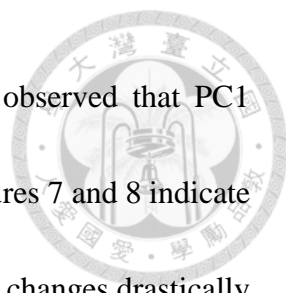
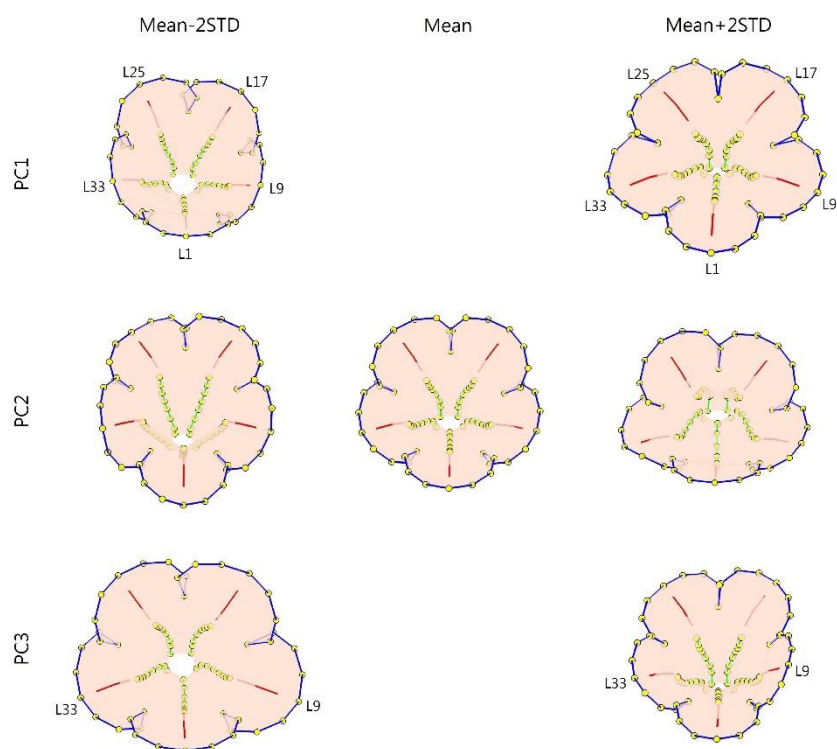
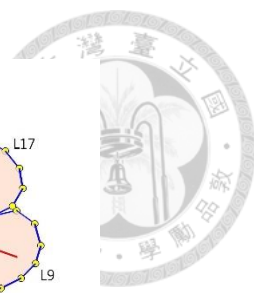


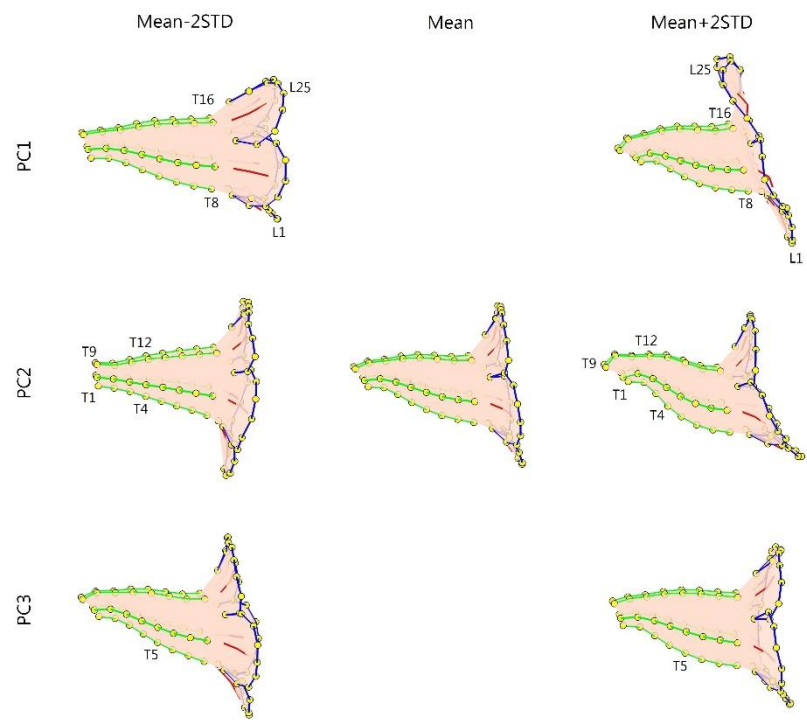
Figure 7. Illustration of flower shape variations caused by changes in PCs.



The shape variation associated with each PC was examined. We observed that PC1 primarily corresponded to corolla curvature and flower opening. Figures 7 and 8 indicate that petal curvature in the boundary region between the lobe and tube changes drastically for the flowers with different PC1 values. The lobes of the flower with a high PC1 value bent outward at a considerable degree (the curves connecting L1-T8 and L25-T16 in Figure 8B). This large curvature produced a wide opening in the flower. The landmarks on lobe contours (from L1 to L33 in Figure 8A) spread out from the center. By contrast, the flower with a low PC1 value was associated with a moderate degree of opening (Figure 8B). In the front-view images, the lobes of the flower with a narrow opening (mean - 2 STD) exhibited a high degree of overlapping compared with the lobes of the flower with a wide opening (mean + 2 STD) in which the lobes were distinctly separated.

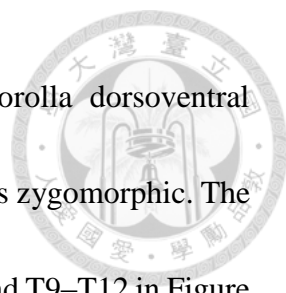


(A)



(B)

Figure 8. (A) Front-view and (B) side-view illustration of the flower shape variations.



We observed that PC2 mainly corresponded to the degree of corolla dorsoventral symmetry (Citerne et al., 2010). The flower with a low PC2 value was zygomorphic. The distances from either side of the petal base (lines connecting T1–T4 and T9–T12 in Figure 8B) to the center of the tube were balanced. By contrast, the flower with a high PC2 value was actinomorphic. The end of the tube (lines connecting T1–T4 and T9–T12) bent upward, resulting in a visible asymmetry between the dorsal and ventral petals. In addition, PC2 corresponded to the degree of overlapping between the ventral and lateral lobes in the front view (Fig. 8A). Compared with the actinomorphic flower, the zygomorphic flower developed a ventral lobe bent downward at a higher degree (Fig. 8B). Because of the aforementioned changes, the flowers with various PC2 values displayed distinct front views (Fig. 8A) for pollinators.

We observed that PC3 particularly corresponded to the size of the tube chamber. The flower with a low PC3 value was associated with a chamber dilated around landmark T5 (Fig. 8B). Furthermore, the flower with a small PC3 value was associated with widely opened lateral lobes (L9 and L33 in Figure 8A).

3.2.3 Morphological traits: flower opening and corolla asymmetry

The GM analysis revealed that flower opening (i.e., corolla curvature) and dorsoventral symmetry were the leading shape variations. Two traits, flower opening and corolla

asymmetry, were defined and identified directly in the 3D flower images. Flower opening was defined as the ratio of the diameters of the lobe-widening circle to the tube-opening circle (Fig. 9A). The lobe-widening circle was defined as the smallest circle that comprised the lobe contour. The tube-opening circle was defined as the optimally fitted circle of the 5 lobe intersections. Corolla asymmetry was defined as the sine value of the asymmetry angle. The asymmetry angle (θ in Figure 9B) was the angle between the long axis of the corolla tube and the normal vector of the tube-opening circle. On the basis of these definitions, the two traits were unaffected by the size, translation, or rotation of the 3D flower images.

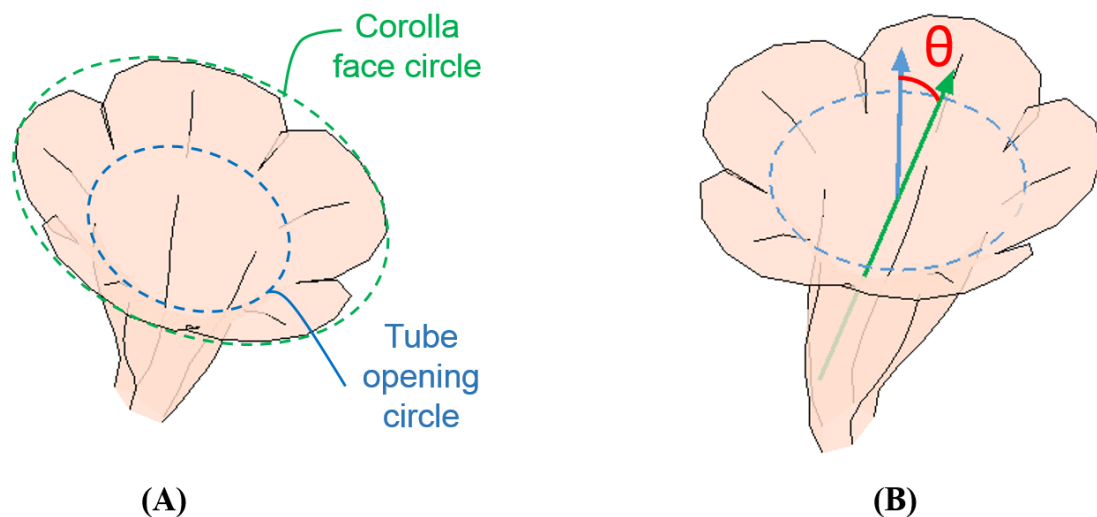


Figure 9. (A) Tube-opening and lobe-widening circles for calculating the opening score and (B) the asymmetry angle.

Analysis was conducted to determine if PC1 and PC2 were linearly correlated to flower opening and corolla asymmetry, respectively. Figure 10 shows the scatter plots of the

analysis. The data were normalized with zero means and unit variances. Moderate correlation was observed. The correlation coefficient between PC1 and the flower opening score was -0.53 , and the correlation coefficient between PC2 and the asymmetry score was 0.61 . This indicates that the two defined flower traits can generally represent the principal shape variations.

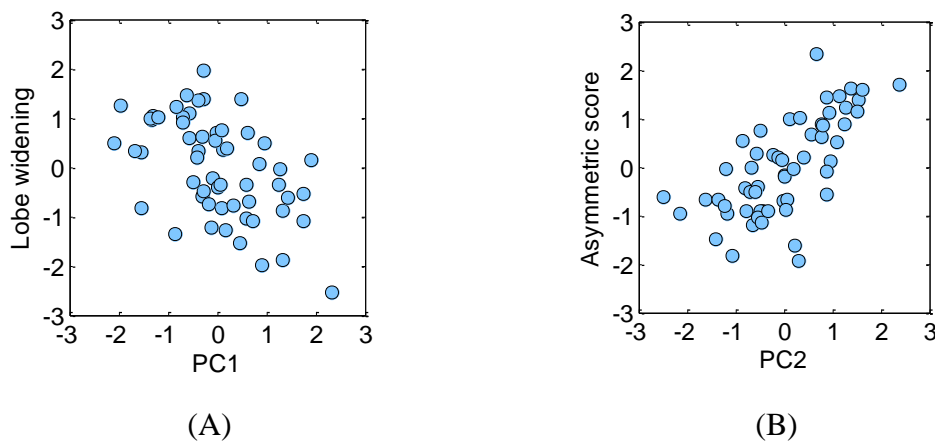


Figure 10. Scatter plots of (A) PC1 and flower opening, and (B) PC2 and the asymmetry score.

3.2.4 Transition between the zygomorphic and actinomorphic flowers

Figure 11 shows the distributions of flower opening and corolla asymmetry. The mean and STD of flower opening were 1.74 and 0.12 , respectively. The mean and STD of corolla asymmetry were 0.07 and 0.28 (the corresponding asymmetry angles were 4.19° and 16.19°), respectively. Figure 11A and 11C show the flower images with extreme flower opening values (1.43 and 1.98). Figures 11D and 11F show the flower images with the extreme corolla asymmetry values (0.14 and 0.44).

The two traits could be unimodally and continuously distributed (Fig. 11). The hypothesis that flower widening and corolla asymmetry were normally distributed could not be rejected by the Kolmogorov–Smirnov test ($P = 0.45$ and 0.49). These observations suggested that a polygenic basis of these traits existed. In addition, the correlation coefficient between the two traits was 0.195 , indicating that the development of these traits were likely independent.

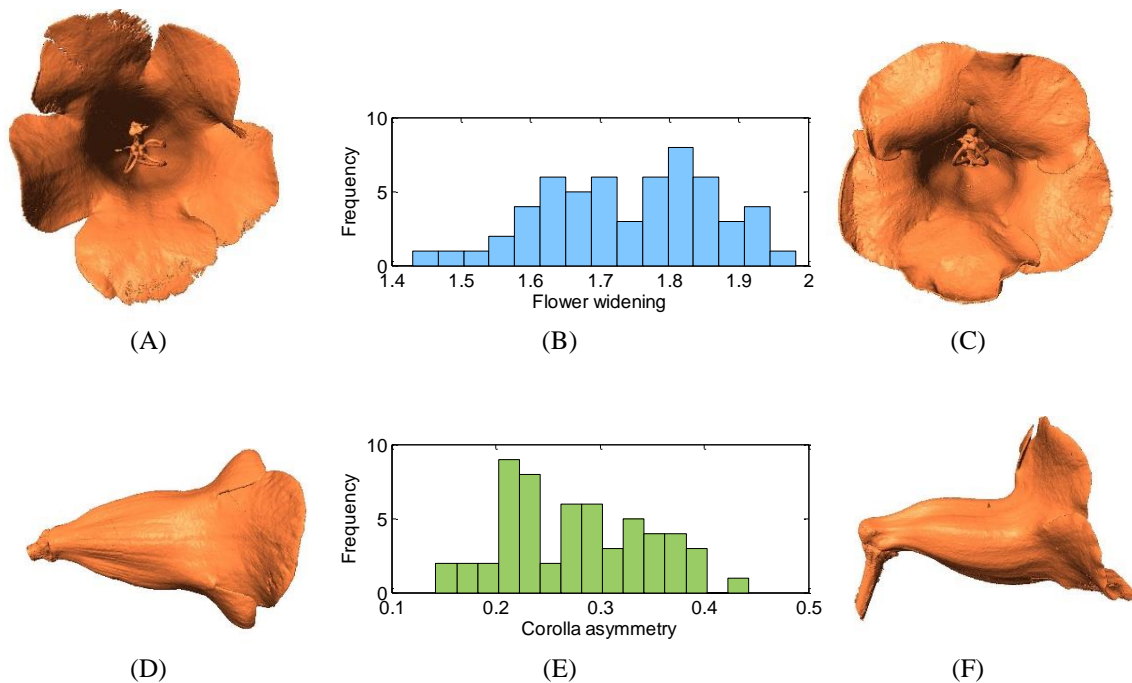


Figure 11. (A) Flower of the smallest opening value, (B) histogram of flower opening, (C) flower of the largest opening value, (D) flower of the smallest corolla asymmetry, (E) histogram of corolla asymmetry, and (F) flower of the largest corolla asymmetry.

3.2.5 Comparison of shape variation analyses performed using 2D and 3D images

The performance of the proposed approach was compared with that of the conventional method, which determines the floral shape variations by using 2D images (Hsu et al.,

2015). The 2D images were obtained by projecting the 3D flower images onto 2D planes. In the projection, the view angle of a flower was set according to its tube-opening circle (Fig. 9A) and dorsoventral planes to capture the front-view and side-view images of the flower (Fig. 12). This projection process mimicked the action of acquiring 2D flower images by using a camera. Subsequently, landmarks were identified on the images by following the procedure stated in a previous study (Hsu et al., 2015). All the front-view landmarks were located on the lobe contours, whereas all the side-view landmarks were located on the tube contours (Fig. 12). This limitation was because of the challenge of accurately determining landmarks on the tubes from front views and on the lobes from side views. Thus, 30 front-view and 15 side-view landmarks were collected for each specimen (Fig. 12).

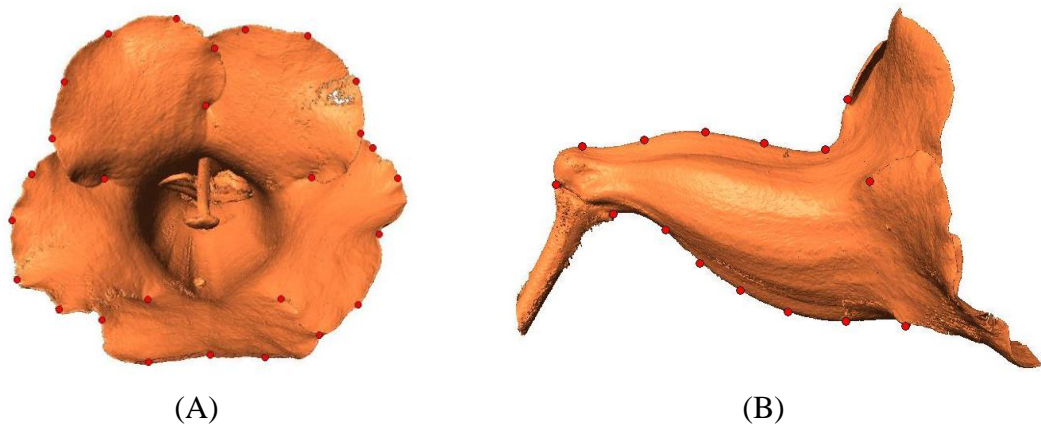



Figure 12. 2D (A) front-view and (B) side-view images of a flower. Red dots indicate landmarks selected along the contours.

To quantify the floral shape variation, two GM analyses were conducted using the front-view and side-view landmarks, respectively. This procedure followed the typical



approach used for 2D images (Kawabata et al., 2009; Hsu et al., 2015). The first two PCs obtained from the front-view landmarks, referred to as F-PC1 and F-PC2, accounted for 19.0% and 14.5% of the total shape variation. The first two PCs obtained from the side-view landmarks, referred to as S-PC1 and S-PC2, accounted for 44.0% and 16.2% of the total shape variation. Figure 13 displays the floral shape variation caused by the changes in the first two PCs. We observed that F-PC1 and F-PC2 primarily corresponded to the ventral lobe extension and the degree of overlapping between the lobes. Furthermore, S-PC1 and S-PC2 principally corresponded to the dorsoventral asymmetry and the opening of the tube chamber. The flower opening (i.e., corolla curvature) characteristic shown in the 3D GM analysis was not observed in the 2D GM analysis.

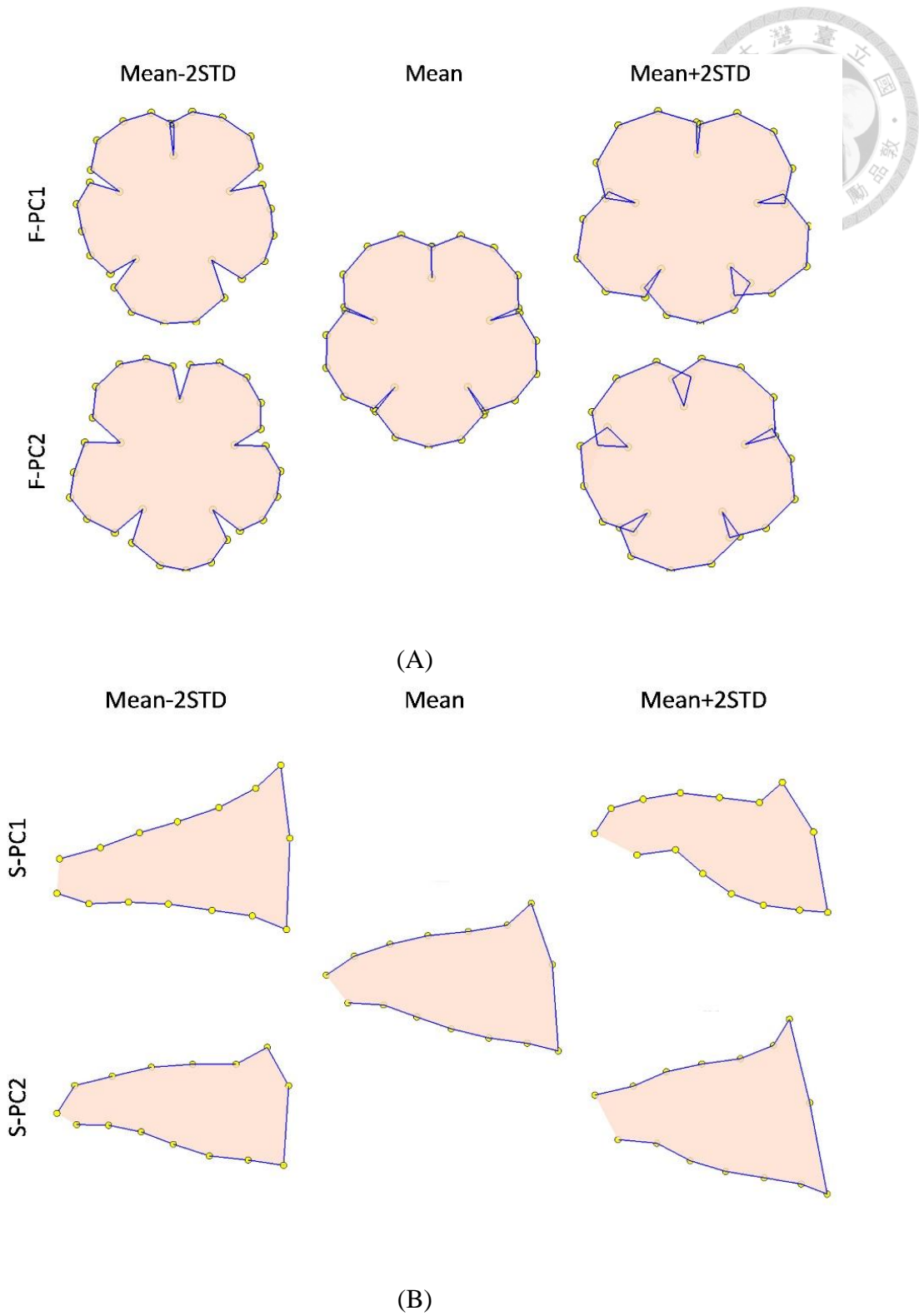


Figure 13. (A) Front-view and (B) side-view illustrations of the floral shape variation quantified using 2D images.



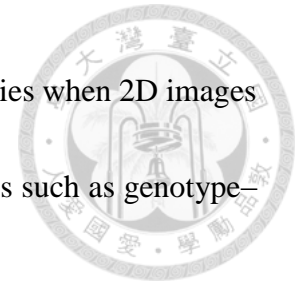
3.4 Discussion

3.4.1 Advantages of 3D floral shape analysis

The 3D analysis explored the additional aspects of the corolla shape variation that was not observed using the conventional 2D methods. Our proposed approach can identify corolla curvature (i.e., flower opening). The 3D GM analysis revealed that the corolla curvature corresponded to the major portion of the total shape variation (i.e., PC1). However, this was not identified by the 2D GM analysis (Fig. 13). Corolla curvature has been demonstrated to act as a mechanical nectar guide, which facilitates direct flower handling for plant–pollinator interactions (Campos et al., 2015). The corolla curvature is perhaps an essential trait for the development and evolution of flower shape

Three-dimensional images enables quantification of flower traits. Flower shape is complex, and the principal shape variations are often presented qualitatively (e.g., GM analysis results). By using 3D images, flower traits corresponding to the leading shape variations can be further defined and measured with high accuracy. In this study, the traits of the corolla, such as the tube-opening circle, lobe-widening circle, and long axis, were quantified. Subsequently, the flower opening and corolla asymmetry scores were derived. These traits of flowers are physically measured and can quantitatively represent the flower shapes. Furthermore, these traits are crucial parameters that illustrate the transition between the zygomorphic and actinomorphic flowers. By contrast, these flower traits


could be difficult to assess or quantify with a high level of uncertainties when 2D images are used. These traits can be used in future studies that address topics such as genotype–phenotype association or plant–pollinator interactions.



Graphics using 3D information are more powerful tools that illustrate flower shapes. With 3D coordinates, the corollas could be observed from various view angles in more detail (e.g., midribs). In addition, the lobe and tube of a corolla could be illustrated together in a 3D image (Fig. 7), whereas a 2D image could only demonstrate the lobe or tube of a corolla (Fig. 13). The partial information obtained in 2D images may result in the misinterpretation of the floral shape variations. For example, the 2D graphical illustration (Fig. 13a) could lead to a false interpretation of the shape variation corresponding to F-PC1 as the degree of overlapping for the ventral lobe, whereas the same shape variation was clearly observed as dorsoventral asymmetry in the 3D graphical illustration (Fig. 7).

3.4.2 Reasons for 3D analysis outperforming 2D analysis

Three-dimensional images inherently contain more anatomical details (e.g., midribs). Landmarks must be situated on the homologous loci in all specimens and are typically identified on the basis of these anatomical details. By contrast, a large portion of geometric details are not available in 2D images. Thus, less shape variations can be quantified using 2D images. In addition, certain 2D landmarks are identified on the lobe



or tube contours (Fig. 12). These contours are projections on 2D planes and are subjected to the view angle of a camera. Thus, uncertainties can be introduced in the contours when the flower images are taken. Subsequently, these uncertainties propagate to the landmark coordinates. Moreover, a 3D flower image comprises both the lobe and tube landmarks of the same flower. The lobe and tube landmarks are subjected to the GM analysis simultaneously; therefore, the association between the two compartments can be retained. However, a 2D image comprises only the lobe or tube landmarks (Fig. 13). Conducting the shape analysis by using only one of the datasets separately leads to a loss of association between the two compartments, therefore failing to retain the inherent shape information.

3.4.3 Biological implications of flower shape variations

Our 3D GM analysis facilitated in identifying the flower opening and corolla asymmetry (indicated by the asymmetry angle) as the two major traits for the petal shape variations in the transition between actinomorphic and zygomorphic flowers. Wide flower opening and bilateral symmetry in the zygomorphic F_2 individuals allow only those pollinators that enter flowers in a certain direction, thus facilitating pollen deposition on these visitors. Narrow flower opening and radial symmetry in the actinomorphic F_2 individuals indicates that the flowers are unable to restrict pollinators entering from any direction. Flowering

plants with bilateral symmetry have been demonstrated greatly in facilitating plant–pollinator interactions or coevolution.



3.5 Concluding Remarks

This chapter proposed procedures to quantify the floral shape variations in 3D by using μ CT, GM, and image processing. The procedures were applied to an F_2 population from interbreeding two cultivars of *S. speciosa* of actinomorphic and zygomorphic flowers. Three-dimensional images determined the floral shape variations as a whole and measured the morphological traits accurately. The proposed 3D- μ CT-GM approach revealed shape variations that could not be identified using typical 2D approaches and accurately quantified the flower traits that presented a challenge in 2D images. This approach has potential for application in future studies on genotype–phenotype associations or evolutionary divergence.

CHAPTER 4. MORPHOLOGICAL INTEGRATION BETWEEN FLORAL PETALS FOR *SINNINGIA SPECIOSA*



This chapter aims to examine the level of morphological integration for flower petals of *S. speciosa*. Morphological integration refers to the tendency of illustrating correlation in shape variation between compartments. In this study, a zygomorphic *S. speciosa* was crossed with an actinomorphic *S. speciosa*. The second-generation flowers from the cross illustrate considerable shape variations, particularly in flower opening and dorsoventral asymmetry mentioned in chapter 3. Landmarks of the flowers were identified to describe the shapes of the petals. Subsequently, the level of morphological integration between the petal landmark sets were examined by using generalized Procrustes analysis and permutation tests. The tests indicated that dorsal and ventral petals were associated with a minimal level of integration and could be regarded as biological modules.



4.1 Materials and Methods

4.1.1 Flower compartments

The landmarks of a corolla were divided into 3 compartments: dorsal, lateral, and ventral petals (Fig. 14). In this study, two sets of compartments were formed. In the first set, the compartments included both the lobe and tube landmarks (Fig. 14A). In the second set, the compartments included only the tube landmarks (Fig. 14B). The lobe illustrated an additional shape variation, flower opening, in a previous study (Hsu et al., 2015). Hence, the lobe landmarks were disregarded in the second compartment set to minimize effect of the flower opening.

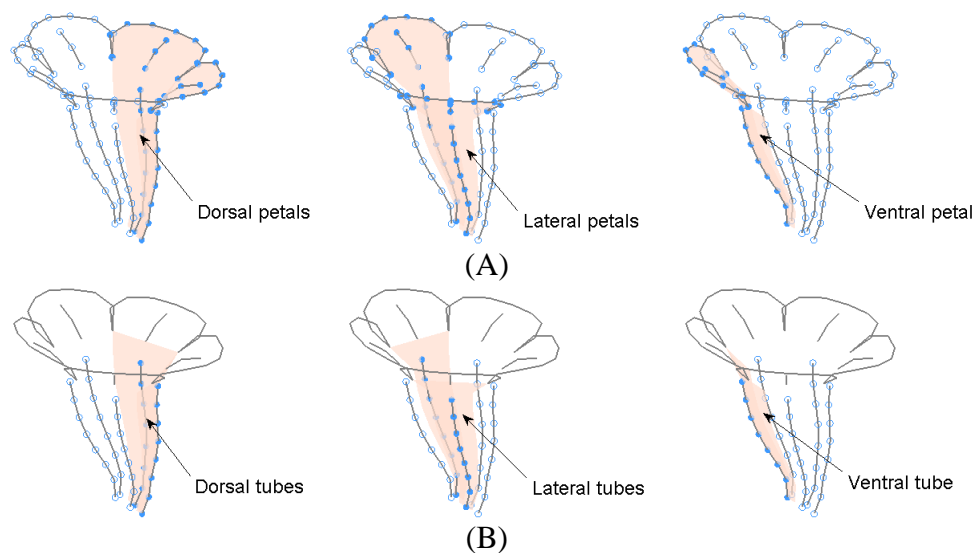
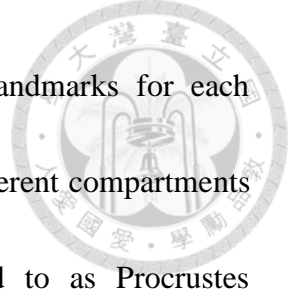


Figure 14. Compartments of landmarks. (A) Compartments of petals (B) compartments of tubes.

General Procrustes analysis (GPA; Gower, 1975) was applied to the landmarks of all the corollas for removing between-flower variation irrelevant to shape (i.e., rotation,



translation, and scaling). Separate GPA was performed to the landmarks for each compartment (Klingenberg, 2009) because the landmark sets of different compartments were not mutually exclusive. The resulting landmarks, referred to as Procrustes landmarks, were in a form of a matrix for each compartment

4.1.2 Test of Morphological Integration

Covariance between two compartments was measured by using Escoufier's RV coefficient (Escoufier, 1973; Klingenberg, 2009). Suppose there exists n corolla specimen. Let $\mathbf{X} \in \mathfrak{R}^{n \times 3p}$ and $\mathbf{Y} \in \mathfrak{R}^{n \times 3q}$ represent the Procrustes landmarks of two compartments to be analyzed, where p and q are numbers of landmarks in the two compartments. The RV coefficient of the two compartments, $RV(\mathbf{X}, \mathbf{Y})$, was defined as the ratio of the covariance of the two Procrustes landmark sets to the square root of the products of the Procrustes landmark variances, i.e.,

$$RV(\mathbf{X}, \mathbf{Y}) = \frac{\text{trace}(\text{Cov}(\mathbf{X}, \mathbf{Y}) \text{Cov}(\mathbf{Y}, \mathbf{X}))}{\sqrt{\text{trace}(\text{Cov}(\mathbf{X})^2) \cdot \text{trace}(\text{Cov}(\mathbf{Y})^2)}} \in \mathfrak{R}, \quad (1)$$

where $\text{Cov}(\mathbf{X})$ and $\text{Cov}(\mathbf{Y})$ are the covariance matrices of \mathbf{X} and \mathbf{Y} respectively.

$\text{Cov}(\mathbf{X}, \mathbf{Y}) = \text{Cov}(\mathbf{Y}, \mathbf{X})'$ is the cross covariance matrix between \mathbf{X} and \mathbf{Y} .

The RV coefficient ranges between zero and one. A zero RV value indicates that no covariance between two compartments, whereas an RV value of one means the variance between two compartments are completely correlated. The RV coefficient was used as the



statistic for the subsequent hypothesis test.

Permutation test (Manly, 2007) was applied to evaluate the level of integration between two compartments. The approach computationally establishes the distribution of a test statistic and then accordingly conducts a hypothesis testing. In the distribution establishment, the corolla numbers on the landmarks of a compartment (e.g., matrix Y) were shuffled. An RV coefficient was computed according to the new dataset. The shuffle procedure was repeated for 10,000 times to establish the null distribution of the RV coefficients. Next, the p-value of a null hypothesis was calculated. The null hypothesis was that the two compartments did not illustrate correlation in shape variation. The p-value of the test was the frequency of the RV coefficients in the null distribution that were equal or greater than the RV coefficient computed from the original Procrustes landmark sets. A low p-value indicates a high level of covariance between two compartments. The permutation test was used because it is a nonparametric approach and the distribution of the RV coefficient is typically unknown.

4.2 Results

4.2.1 Morphological integration

Figure 15 shows the null distributions of the permutation tests for the first compartment set (petal; Fig. 14A). The red arrows indicate the RV coefficients computed using the

original Procrustes landmark sets. The tests indicated the assumption that the dorsal and ventral petals were not correlated in shape variation could not be rejected ($P > 0.01$).

Figure 16 shows the null distributions of the permutation tests for the second compartment set (tube only; Fig. 14B). The tests indicated that the null hypothesis that the dorsal—ventral and lateral—ventral tubes were not correlated in shape variation could not be rejected ($P > 0.01$). It can be observed that the RV coefficients calculated from the original Procrustes landmark sets for the petals (e.g., first compartment set) are larger than the RV coefficients for the tubes (e.g., second compartment set). This is because the flower opening (Hsu et al., 2015) is a common shape variation among all the lobes. Including lobe landmarks in the permutation analysis increases the covariance between the petals. This observation suggested that including only the tube landmarks for analyzing morphological integration of corollas can be a more appropriate operation.

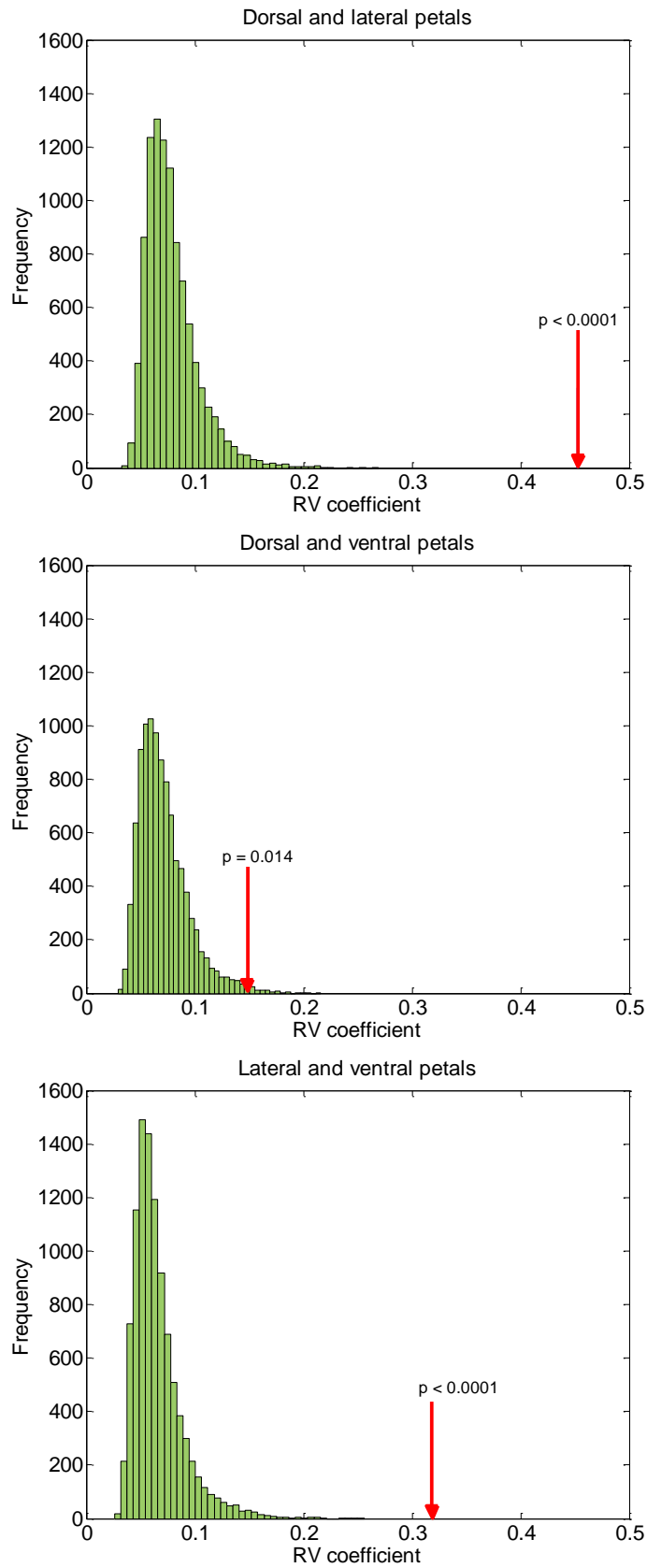


Figure 15. Null distributions of the permutation tests for first compartment set.

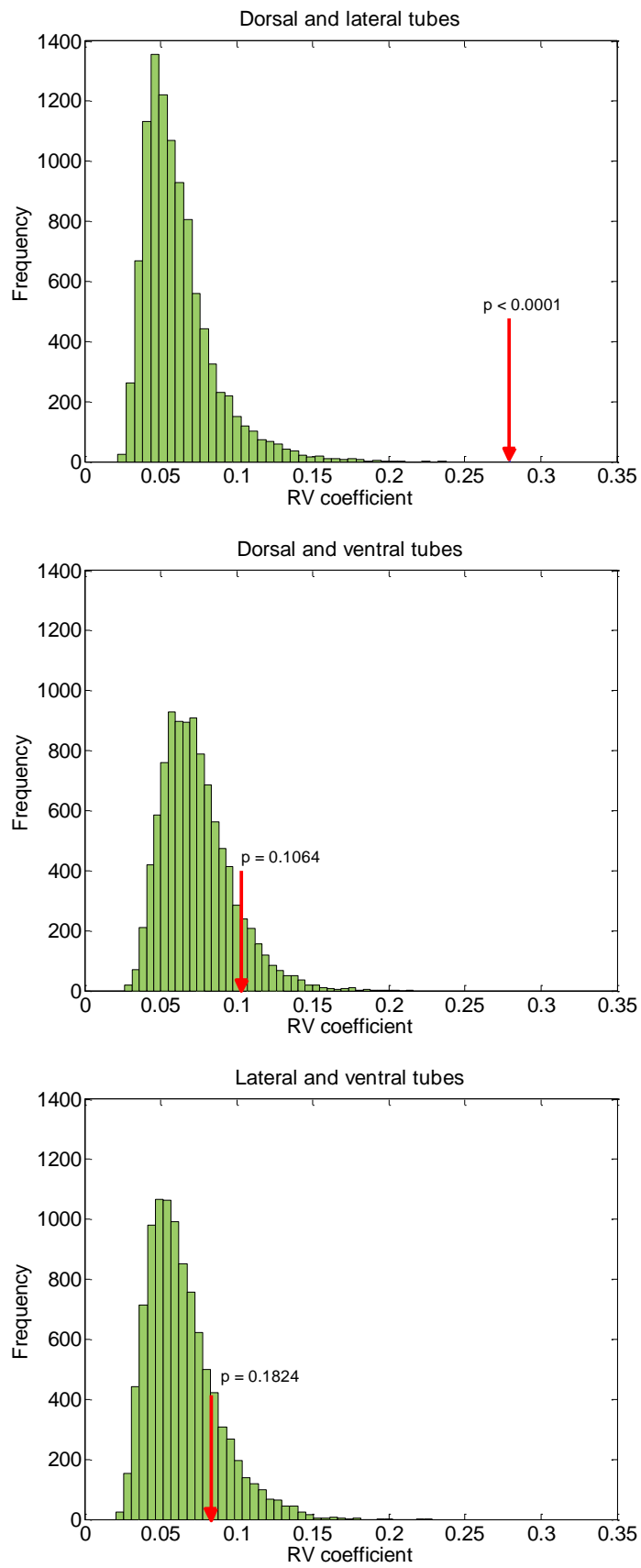


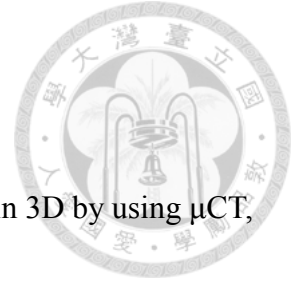
Figure 16. Null distributions of the permutation tests for second compartment set.

4.3 Concluding Remarks

This chapter examined the level of morphological integration between flower petals of *S. speciosa*. The high-resolution of μ CT makes it possible to describe the petal shapes precisely. The analysis indicated that the level of integration between dorsal and ventral petals were minimal. Hence, the dorsal and ventral petals can be regarded as biological modules.



CHAPTER 5. CONCLUSIONS



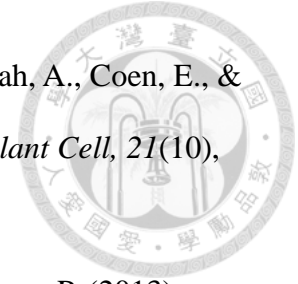
This study aimed to quantify and analyze the floral shape variations in 3D by using μ CT, GM, and image processing. In chapter 3, the high-resolution 3D images using μ CT makes it possible to quantify the flower shapes precisely. Landmarks were identified from the 3D images and then were subjected to GM analysis. GM showed that PC1 represented the corolla curvature and flower opening. PC2 represented the degree of corolla dorsoventral symmetry. PC3 corresponded to the size of the tube chamber. The 3D image analysis revealed shape variations that could not be identified using typical 2D approaches. Therefore, the 3D images accurately quantified the flower traits that presented a challenge in 2D images. In chapter 4, the analysis of integration of flower petals for *S.speciosa* were examined. The landmarks of a corolla were divided into 3 compartments: dorsal, lateral, and ventral petals. The results of permutation test indicated that the level of integration between dorsal and ventral petals were minimal. Hence, the dorsal and ventral petals can be regarded as biological modules.

REFERENCES



- Adams, D. C., Rohlf, F. J., & Slice, D. E. (2004). Geometric morphometrics: ten years of progress following the 'revolution'. *Italian Journal of Zoology*, 71(1), 5-16.
- Bo, W., Wang, Z., Xu, F., Fu, G., Sui, Y., Wu, W., Zhu, X., Yin, D., Yan, Q., & Wu, R. (2014). Shape mapping: genetic mapping meets geometric morphometrics. *Brief Bioinform*, 15(4), 571-581.
- Bookstein, F. L., Gunz, P., Mitterøcker, P., Prossinger, H., Schæfer, K., & Seidler, H. (2003). Cranial integration in *Homo*: singular warps analysis of the midsagittal plane in ontogeny and evolution. *Journal of Human Evolution*, 44(2), 167-187.
- Campos, E. O., Bradshaw, H. D., & Daniel, T. L. (2015). Shape Matters: corolla curvature improves nectar discovery in the hawkmoth *Manduca sexta*. *Functional Ecology*, 29(4), 462-468.
- Citerne, H., Jabbour, F., Nadot, S., & Damerval, C. (2010). The Evolution of Floral Symmetry. *Advances in Botanical Research*, 54, 85-137.
- Cui, M. L., Copsey, L., Green, A. A., Andrew Bangham, J., & Coen, E. (2010). Quantitative control of organ shape by combinatorial gene activity. *PLoS Biology*, 8(11).
- Dalayap, R. M., Torres, M. A. J., & Demayo, C. G. (2011). Landmark and outline methods in describing petal, sepal and labellum shapes of the flower of Mokara orchid varieties. *International Journal of Agriculture and Biology*, 13(5), 652-658.
- Escoufier, Y. (1973). Le traitement des variables vectorielles. *Biometrics*, 29(4), 751-760.

Feng, X., Wilson, Y., Bowers, J., Kennaway, R., Bangham, A., Hannah, A., Coen, E., & Hudson, A. (2009). Evolution of allometry in *Antirrhinum*. *Plant Cell*, 21(10), 2999-3007.



Fernández-Mazuecos, M., Blanco-Pastor, J. L., Gómez, J. M., & Vargas, P. (2013).

Corolla morphology influences diversification rates in bifid toadflaxes (*Linaria* sect. *Versicolores*). *Annals of botany*, 112(9), 1705-1722.

Gómez, J. M., Perfectti, F., & Camacho, J. P. M. (2006). Natural selection on *Erysimum mediohispanicum* flower shape: insights into the evolution of zygomorphy. *The American Naturalist*, 168(4), 531-545.

Galliot, C., Stuurman, J., & Kuhlemeier, C. (2006). The genetic dissection of floral pollination syndromes. *Current Opinion in Plant Biology*, 9(1), 78-82.

Gomez, J. M., Bosch, J., Perfectti, F., Fernandez, J. D., Abdelaziz, M., & Camacho, J. P. (2008). Spatial variation in selection on corolla shape in a generalist plant is promoted by the preference patterns of its local pollinators. *Proceedings of the Royal Society of London, Series B: Biological Sciences*, 275(1648), 2241-2249.


Gower, J. C. (1975). Generalized Procrustes analysis. *Psychometrika*, 40(1), 33-51.

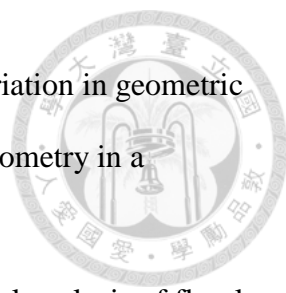
Hansen, C. D., & Johnson, C. R. (2005). *The visualization handbook*: Academic Press.


Haralick, R. M., & Shapiro, L. G. (1992). *Computer and Robot Vision* (2 Ed. Vol. 1). New York: Addison-Wesley.


Hsu, H.-C., Chen, C.-Y., Wang, C.-N., Lee, T.-K., Weng, L.-K., Kuo, Y.-F., & Lin, T.-T. (2015). Quantitative Analysis of Floral Symmetry and Tube Dilation in an F2 Cross of *Sinningia Speciosa*. *Scientia Horticulturae*, 188, 71-77.

Jamniczky, H. A., & Hallgrímsson, B. (2011). Modularity in the skull and cranial vasculature of laboratory mice: implications for the evolution of complex phenotypes. *Evolution and Development*, 13(1), 28-37.

- 
- Kaczorowski, R. L., Seliger, A. R., Gaskett, A. C., Wigsten, S. K., & Raguso, R. A. (2012). Corolla shape vs. size in flower choice by a nocturnal hawkmoth pollinator. *Functional Ecology*, 26(3), 577-587.
- Kanaya, T., Watanabe, H., Kokubun, H., Matsubara, K., Hashimoto, G., Marchesi, E., Bullrich, L., & Ando, T. (2010). Current status of commercial *Calibrachoa* cultivars as assessed by morphology and other traits. *Scientia Horticulturae*, 123(4), 488-495.
- Kawabata, S., Yokoo, M., & Nii, K. (2009). Quantitative analysis of corolla shapes and petal contours in single-flower cultivars of lisianthus. *Scientia Horticulturae*, 121(2), 206-212.
- Kawabata, S., Nii, K., & Yokoo, M. (2011). Three-dimensional formation of corolla shapes in relation to the developmental distortion of petals in *Eustoma grandiflorum*. *Scientia Horticulturae*, 132(1), 66-70.
- Klingenberg, C. P., & Zaklan, S. D. (2000). Morphological integration between developmental compartments in the *Drosophila* wing. *Evolution*, 54(4), 1273-1285.
- Klingenberg, C. P., Badyaev, A. V., Sowry, S. M., & Beckwith, N. J. (2001). Inferring developmental modularity from morphological integration: analysis of individual variation and asymmetry in bumblebee wings. *The American Naturalist*, 157(1), 11-23.
- Klingenberg, C. P. (2009). Morphometric integration and modularity in configurations of landmarks: tools for evaluating a priori hypotheses. *Evolution and Development*, 11(4), 405-421.
- Klingenberg, C. P. (2010). Evolution and development of shape: integrating quantitative approaches. *Nature Reviews Genetics*, 11(9), 623-635.

- 
- Klingenberg, C. P., & Marugán-Lobón, J. (2013). Evolutionary covariation in geometric morphometric data: analyzing integration, modularity, and allometry in a phylogenetic context. *Systematic Biology*, 62(4), 591-610.
- Kobayashi, K., Horisaki, A., Niikura, S., & Ohsawa, R. (2007). Diallel analysis of floral morphology in radish (*Raphanus sativus* L.). *Euphytica*, 158(1-2), 153-165.
- Kuhl, F. P., & Giardina, C. R. (1982). Elliptic Fourier features of a closed contour. *Computer graphics and image processing*, 18(3), 236-258.
- Lawing, A. M., & Polly, P. D. (2010). Geometric morphometrics: recent applications to the study of evolution and development. *Journal of Zoology*, 280(1), 1-7.
- Li, X., Pan, Z., Upadhyaya, S. K., Atungulu, G. G., & Delwiche, M. (2011). *Three-dimensional geometric modeling of processing tomatoes*. Paper presented at the ASABE.
- Manly, B. F. J. (2007). *Randomization, Bootstrap and Monte Carlo Methods in Biology* (3 ed.). London: Chapman and Hall.
- McElrone, A. J., Choat, B., Parkinson, D. Y., MacDowell, A. A., & Brodersen, C. R. (2013). Using high resolution computed tomography to visualize the three dimensional structure and function of plant vasculature. *Journal of Visualized Experiments*(74).
- Miller, J. S., & Venable, D. L. (2003). Floral morphometrics and the evolution of sexual dimorphism in *Lycium* (Solanaceae). *Evolution*, 57(1), 74-86.
- Mitteroecker, P., & Bookstein, F. (2008). The evolutionary role of modularity and integration in the hominoid cranium. *Evolution*, 62(4), 943-958.
- Nii, K., & Kawabata, S. (2011). Assessment of the association between the three-dimensional shape of the corolla and two-dimensional shapes of petals using

- 
- Fourier descriptors and principal component analysis in *Eustoma grandiflorum*.
Journal of the Japanese Society for Horticultural Science, 80(2), 200-205.
- Olson, E. C., & Miller, R. L. (1958). *Morphological integration*. Chicago: University of Chicago Press.
- Pérez, R., Vargas, P., & Arroyo, J. (2004). Convergent evolution of flower polymorphism in *Narcissus* (Amaryllidaceae). *New Phytologist*, 161(1), 235-252.
- Pajor, R., Fleming, A., Osborne, C. P., Rolfe, S. A., Sturrock, C. J., & Mooney, S. J. (2013). Seeing space: visualization and quantification of plant leaf structure using X-ray micro-computed tomography. *Journal of Experimental Botany*, 64(2), 385-390.
- Rohlf, F. J., & Slice, D. (1990). Extensions of the Procrustes method for the optimal superimposition of landmarks. *Systematic Biology*, 39(1), 40-59.
- Savriama, Y., Gómez, J. M., Perfectti, F., & Klingenberg, C. P. (2012). Geometric morphometrics of corolla shape: dissecting components of symmetric and asymmetric variation in *Erysimum mediohispanicum* (Brassicaceae). *New Phytologist*, 196(3), 945-954.
- Shipunov, A. B., Fay, M. F., Pillon, Y., Bateman, R. M., & Chase, M. W. (2004). *Dactylorhiza* (Orchidaceae) in European Russia: combined molecular and morphological analysis. *American Journal of Botany*, 91(9), 1419-1426.
- van der Niet, T., Zollikofer, C. P., Leon, M. S., Johnson, S. D., & Linder, H. P. (2010). Three-dimensional geometric morphometrics for studying floral shape variation. *Trends Plant Sci*, 15(8), 423-426.
- Vincent, L. (1994). Morphological area openings and closings for grey-scale images *Shape in Picture* (pp. 197-208): Springer Berlin Heidelberg.

- 
- Wessinger, C. A., Hileman, L. C., & Rausher, M. D. (2014). Identification of major quantitative trait loci underlying floral pollination syndrome divergence in *Penstemon*. *Philos Trans R Soc Lond B Biol Sci*, 369(1648).
- Wiley, D. F., Amenta, N., Alcantara, D. A., Ghosh, D., Kil, Y. J., Delson, E., Harcourt-Smith, W., Rohlf, F. J., St John, K., & Hamann, B. (2005). *Evolutionary morphing*. Paper presented at the Visualization, 2005. VIS 05. IEEE.
- Yoshioka, Y., Iwata, H., Ohsawa, R., & Ninomiya, S. (2005). Quantitative evaluation of the petal shape variation in *Primula sieboldii* caused by breeding process in the last 300 years. *Heredity*, 94(6), 657-663.
- Yoshioka, Y., Iwata, H., Hase, N., Matsuura, S., Ohsawa, R., & Ninomiya, S. (2006). Genetic Combining Ability of Petal Shape in Garden Pansy (*Viola × wittrockiana* Gams) based on Image Analysis. *Euphytica*, 151(3), 311-319.
- Yoshioka, Y., Ohashi, K., Konuma, A., Iwata, H., Ohsawa, R., & Ninomiya, S. (2007). Ability of bumblebees to discriminate differences in the shape of artificial flowers of *Primula sieboldii* (Primulaceae). *Ann Bot*, 99(6), 1175-1182.
- Zelditch, M., Swiderski, D., Sheets, D., & Fink, W. (2004). *Geometric morphometrics for biologists: a primer*. London: Elsevier Academic Press.